



Surface and catalyst driven singlet oxygen formation in Li-O₂ cells

Aleksej Samojlov^a, David Schuster^a, Jürgen Kahr^b, Stefan A. Freunberger^{a,c,*}



^a Institute for Chemistry and Technology of Materials, Graz University of Technology, Stremayrgasse 9, 8010 Graz, Austria

^b Austrian Institute of Technology, Giefinggasse 2, 1210 Wien, Austria

^c IST Austria (Institute of Science and Technology Austria), Am Campus 1, 3400 Klosterneuburg, Austria

ARTICLE INFO

Article history:

Received 20 April 2020

Revised 15 September 2020

Accepted 21 September 2020

Available online 25 September 2020

Keywords:

Li-O₂ batteries

Electrocatalysis

Singlet oxygen

Superoxide

Peroxide

ABSTRACT

Large overpotentials upon discharge and charge of Li-O₂ cells have motivated extensive research into heterogeneous solid electrocatalysts or non-carbon electrodes with the aim to improve rate capability, round-trip efficiency, and cycle life. These features are equally governed by parasitic reactions, which are now recognized to be caused by formation of the highly reactive singlet oxygen (¹O₂). However, the link between the presence of electrocatalysts and ¹O₂ formation in metal-O₂ cells is unknown. Here, we show that, compared to pristine carbon black electrodes, a representative selection of electrocatalysts or non-carbon electrodes (noble metal, transition metal compounds) may both slightly reduce or severely increase the ¹O₂ formation. The individual reaction steps, where the surfaces impact the ¹O₂ yield are deciphered, showing that ¹O₂ yields from superoxide disproportionation as well as the decomposition of traces of H₂O₂ are sensitive to catalysts. Transition metal compounds in general are prone to increase ¹O₂. The results highlight the importance of ¹O₂ in metal-O₂ cells and to use a comprehensive set of metrics to judge the impact of catalysts on reversibility.

© 2020 The Author(s). Published by Elsevier Ltd.

This is an open access article under the CC BY-NC-ND license

(<http://creativecommons.org/licenses/by-nc-nd/4.0/>)

1. Introduction

The quest for electrochemical energy storage with higher energy, lower cost and better ecological footprint compared to the best performing current technology, lithium-ion batteries, motivates research into aprotic lithium-oxygen (Li-O₂) batteries. They operate by reducing O₂ in a porous electrode to form Li₂O₂ upon discharge and its decomposition to evolve O₂ upon recharge [1–7]. Practically realizing such cells faces, however, a number of interconnected challenges. First, the insulating nature of Li₂O₂ hampers fully filling the pores (causing lower than theoretical capacity) and completely decomposing the Li₂O₂ on charge even at low rates [1,5,8–11]. Low rate capability has further been ascribed to sluggish O₂ reduction and evolution reactions. Second, severe parasitic reactions, which decompose cell components and cause poor rechargeability, efficiency, and cycle life [5,7,12,13]. Phenomenologically, these issues cause even at moderate rates of <100 μA cm² geometric large overpotentials with typical values relative to E_{O₂/Li₂O₂} = 2.96 V being ≈0.3 V on discharge and on charge ever rising values as charging proceeds from close to zero to, in some

cases, up to 2 V. Parallels with aqueous O₂ electrochemistry motivated the use of electrocatalysts, which have been broadly investigated for Li-O₂ cells [1,3,14–24]. However, true impacts of catalysts on reaction rates, underlying mechanisms or even parasitic chemistry are controversial.

Early work suggested (principal) inactivity of solid catalyst on the electrochemistry of micrometre-sized Li₂O₂ particles that cover the catalyst [23]. This is because the insulating Li₂O₂ would passivate any catalyst activity beyond a few monolayers of Li₂O₂. Later works suggested catalysts to act, e.g., via doping of the Li₂O₂, which would make the Li₂O₂ more conductive. More recently, solid-solid catalysis was more deeply explained via formation of intermetallic phases or by reducing the barriers to form solid superoxide-like intermediates through which the charge process passes [3,15,18,19]. Less settled is the role of catalysts in parasitic reactions. Catalysts that do reduce recharge voltage are now recognized to worsen in tendency the O₂ recovery and CO₂ evolution, which are indicators for parasitic reactions [14,20,25]. Particularly at potentials around 4 V and above, such catalysts were noted to non-selectively catalyse oxidation reactions [14,20]. The majority of parasitic reactions is now firmly established to be caused by formation of the highly reactive singlet oxygen (¹O₂) with relatively small extent on discharge and much larger and growing extent from the onset of charge and growing charge potential [17,26–

* Corresponding author. IST Austria (Institute of Science and Technology Austria), Am Campus 1, Klosterneuburg 3400, Austria.

E-mail address: stefan.freunberger@ist.ac.at (S.A. Freunberger).

30]. However, the link between catalyst and the $^1\text{O}_2$ formation in metal- O_2 cells is unknown.

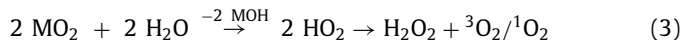
$^1\text{O}_2$ formation in metal- O_2 cells has been identified to either stem from disproportionation or direct electron transfer [27,28,31,32]. We have previously shown that alkali superoxide disproportionation to the peroxide ($\text{M} = \text{Li}, \text{Na}$)



is the major $^1\text{O}_2$ forming step upon discharge and charge in metal- O_2 cells [28]. Hereby, the ${}^1\text{O}_2$ fraction sensitively depends on the $\text{M}^+ - \text{O}_2^-$ ion pairing, which is strongly influenced by the Lewis acidity of M^+ . Discharge commences with one-electron O_2 reduction to superoxide (MO_2), which further disproportionates according to Eq. (1). Similarly, on charge a superoxide intermediate forms by one-electron oxidation of M_2O_2



MO_2 could either be a Li-deficient M_{2-x}O_2 phase or solid, adsorbed, or dissolved MO_2 [10,11,33,34]. In either case, it was shown experimentally and/or theoretically to disproportionate [11,34–39]. Equally, this is the source of ${}^1\text{O}_2$ on charge according to Eq. (1). We do not exclude ${}^1\text{O}_2$ from direct electrochemical oxidation of LiO_2 , which could give ${}^1\text{O}_2$ beyond $E_{\text{O}_2/\text{LiO}_2}^0 + E({}^1\text{O}_2 \leftarrow {}^3\text{O}_2) \sim 3.56 \text{ V}$. However, previous work on the recharge mechanism has shown that at least up to $\sim 3.95 \text{ V}$ disproportionation appears to be the dominant O_2 evolving step [11,28]. An additional source of ${}^1\text{O}_2$ could be proton mediated superoxide disproportionation, e.g., with traces of water [29,40–42]:



H_2O_2 has been shown to form as by-product in metal- O_2 cells in presence of traces of water or other proton sources [9,43,44]. H_2O_2 is well established to catalytically decompose according to $\text{H}_2\text{O}_2 \xrightarrow{\text{cat}} \text{H}_2\text{O} + \frac{1}{2} \text{O}_2$ in contact with mineral compounds [45–47], of which some were shown to partly form ${}^1\text{O}_2$ [47].

Here, we show that the solid surfaces in the electrode (carbons, electrocatalysts) impact the ${}^1\text{O}_2$ formation both on discharge and charge in a similar manner. We used a representative selection of widely used catalyst classes comprising carbon, noble metal, and transition metal compounds. The catalyst's effect on ${}^1\text{O}_2$ formation could potentially stem from its impact on one or more of the intermediate reaction steps discussed above. We show that transition metal oxides enhance the formation of ${}^1\text{O}_2$ from superoxide disproportionation ($2 \text{LiO}_2 \rightarrow \text{Li}_2\text{O}_2 + \text{O}_2$) while (semi)conducting materials reduce ${}^1\text{O}_2$ compared to disproportionation in absence of a catalyst. Catalysts impact, however, the overall ${}^1\text{O}_2$ formation in the $\text{Li}-\text{O}_2$ cell most severely by the fraction of ${}^1\text{O}_2$ they evolve by decomposing traces of H_2O_2 .

2. Experimental

Lithium bis(trifluoromethane)sulfonimide (LiTFSI, 99.9%, Solvionic) was dried under reduced pressure for 24 h at 140°C. Tetraethylene glycol dimethyl ether (TEGDME, ≥99%, Aldrich) was dried over lithium, distilled under Ar and further dried and stored over activated molecular sieves. The water content was determined by Karl-Fisher titration and found to be below 5 ppm. 9,10-Dimethylanthracene (DMA, >98.0 %, Aldrich) was recrystallized from ethanol and its purity confirmed by $^1\text{H-NMR}$ spectroscopy and HPLC analysis. Formic acid was from Fluka (p.a. ~98%). Acetonitrile (HiPerSolv Prolabo) was from VWR. KO_2 was from ABCR and its purity determined using UV-Vis and MS [48]. TiC was from Skyspring nanomaterials and had 40 nm particle size. Pd on carbon was from Sigma Aldrich with 5 wt% loading on

activated carbon. High purity oxygen (O_2 3.5, >99.95 vol%), high purity Ar 5.0 were from Messer Austria. LiFePO_4 was from MTI and partly delithiated according to [49]. Super P was from Timcal. Co_3O_4 and $\alpha\text{-MnO}_2$, respectively, on Super P with a weight ratio of 3/7 were synthesized according to the procedures in [50] and [51] and their purity and identity confirmed by XRD. To make Super P hydrophilic, the as-received carbon was refluxed with 5 M HNO_3 for 24 hours, then filtered and washed with copious amounts of distilled water until the pH of the water was 7.

Carbon cathodes were made with a slurry of the electrode material (carbon, carbon with catalyst, or TiC) with PTFE binder in the ratio 9:1 (m/m) using isopropanol. The slurry was then coated onto a stainless steel mesh current collector. The electrodes were vacuum dried at 200°C for 24 h and then transferred to an Ar filled glove box without exposure to air. The glass fibre separators (Whatman) were washed with ethanol and dried overnight at 200°C under vacuum prior to use. The $\text{Li}_{1-x}\text{FePO}_4$ counter electrodes were made by mixing partially delithiated active material with Super P and PTFE in the ratio 8:1:1(m/m) with isopropanol. The electrodes were vacuum dried at 200°C for 24 h. The counter electrodes had three-fold the expected capacity of the positive electrode. The electrochemical cells used for cycling were of the type EL-Cell PAT-Cell-Press (EL-Cell, Hamburg, Germany). Typical working electrodes had a mass loading of 1 mg and the cells were assembled with 70 μL electrolyte. The electrolyte was 0.1 M LiTFSI in TEGDME containing 3×10^{-2} M 9,10-dimethylanthracene as ${}^1\text{O}_2$ trap. To obtain the amount of ${}^1\text{O}_2$ formed during discharge, an average of at least three cells was taken. An MPG-2 or SP-150 potentiostat/galvanostat (BioLogic, France) was used for electrochemical cycling. Oxidation stability of DMA at the various catalyst was measured by dipping working electrodes into a TEGDME solution containing 0.1 M LiTFSI and 2 mM DMA and measuring linear scan voltammograms at 20 mV s $^{-1}$. Reference and counter electrodes were LiFePO_4 .

UV-Vis absorption spectra were recorded on a Cary 50 spectrophotometer (Varian). Fluorescence measurements were recorded on a Fluorolog 3 fluorescence spectrometer (Horiba) equipped with a NIR-sensitive photomultiplier R2658 (300–1050 nm) from Hamamatsu. The *operando* fluorescence measurements were performed in the front face mode in kinetic acquisition mode with 0.1 s excitation every 10 s to minimize photobleaching of the DMA. Further details of the setup are given in [27]. The electrolyte was 0.1 M LiTFSI in TEGDME containing 1.6×10^{-5} M DMA as ${}^1\text{O}_2$ trap. The mass spectrometry (MS) setup was built in-house and was described in more detail previously [27]. The sample setup consisted of a glass vial with a volume of 7 mL equipped with a stirring bar (Fig. S1) [48]. A PEEK plug with glued in PEEK tubes and a septum is sealed against the glass vial with a flat rubber seal, which are all pressed by an Al clamp. Reagents were added through a septum using a gas tight syringe (Hamilton) and the gas flow was regulated using a four-way valve (Hamilton). All solutions were degassed with N_2 to remove dissolved CO_2 and O_2 . The headspace was purged to the MS using 5 $\text{mL} \cdot \text{min}^{-1}$ Ar 6.0. For monitoring pressure, a high-precision pressure transducer (Omega, PAA35X) was connected to the closed vessel instead of the MS. Reagents were added with a gas tight syringe through glued-in tubing (Hamilton).

For reactions with KO_2 , ~2 mg KO_2 were dissolved together with an equimolar amount of 18-crown-6 in 1 mL TEGDME containing 30 mM DMA and placed together with 2 mg catalyst in the setup described above, connected to either MS or pressure transducer. Then either 1 mL TEGDME containing 0.1 M LiTFSI, 30 mM DMA or 1 mL TEGDME containing 2000 ppm H_2O_2 and 30 mM DMA were added. For reactions with H_2O_2 , 35% H_2O_2 in H_2O were mixed with TEGDME containing 30 mM DMA to obtain a 170 mM H_2O_2 solution. This solution was injected into the setup

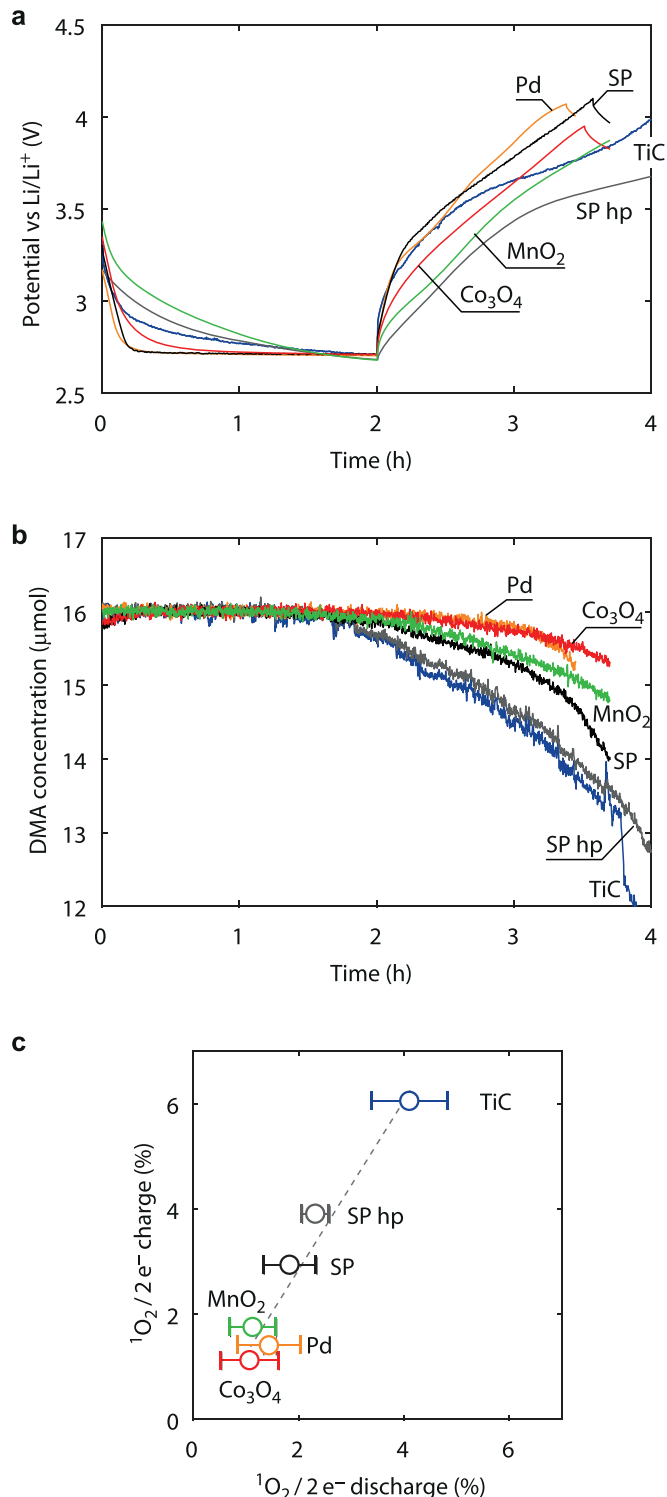


Fig. 1. $^1\text{O}_2$ generation during discharge and charge in presence of different catalysts/carbons. (a,b) Operando fluorescence spectroscopy during Li-O₂ cell operation. Voltage (a) and evolution of the DMA concentration (b) during galvanostatic discharge and charge at $\sim 16 \mu\text{A}\cdot\text{cm}^{-2}$. (c) Detected amount of $^1\text{O}_2$ normalized to the charge passed upon discharge with above electrodes.

with pressure transducer with 2 mg catalyst placed already inside. H₂O₂ concentration was measured using 2 wt% solution of Ti(IV)-oxysulfate solution in 1 M H₂SO₄ and measuring the absorbance of the Ti-peroxy complex at 405 nm.

High-performance liquid chromatography (HPLC) was used to determine the degree of the DMA to DMA-O₂ conversion as de-

scribed earlier [27]. The filtered electrolyte was diluted with DME to $\sim 1 \text{ mg}_{\text{DMA}}\cdot\text{mL}^{-1}$ and a volume of 2 μL was injected into the HPLC. The HPLC instrument was a 1200 Series (Agilent Technology). The eluent was monitored via an UV-Vis detector (Agilent Technology G1365C MWD SL) at 210 nm. The samples were analysed by a reversed-phase column (Poroshell 120 EC-C8, 3.0 mm \times 100 mm, Ø 2.7 μm , Agilent Technology) using a gradient system of acetonitrile (solvent B) and water containing 0.01% formic acid (solvent A). A pre-column (UHPLC 3PK, Poroshell 120 EC-C8 3.0 mm \times 5 mm, Ø 2.7 μm , Agilent Technology) was connected before the reversed-phase column. The elution at a flow rate of 0.7 mL/min started with 50% solvent B and was then increased to 100% solvent B. The extent of the transformation of DMA to DMA-O₂ conversion was determined from the absorbance at 210 nm and the molar absorption coefficients $\epsilon_{\text{DMA}, 210\text{nm}}$ and $\epsilon_{\text{DMA-O}_2, 210\text{nm}}$. The latter was determined from DMA-O₂, which was obtained by conversion of DMA with photogenerated $^1\text{O}_2$ [27,52].

3. Results and discussion

To detect $^1\text{O}_2$ formation, we used the previously established method using 9,10-dimethylanthracene (DMA), which rapidly and selectively traps $^1\text{O}_2$ by forming its endoperoxide (DMA-O₂). Both DMA and DMA-O₂ are electrochemically stable in the required potential range between ~ 2 and 4.1 V. Further, DMA-O₂ does not form in presence of other possible reactive oxygen species such as O₂, superoxide, or peroxide [27,31,53]. DMA-O₂ formation due to the presence of $^1\text{O}_2$ can then either be detected by following the change of absorbance or fluorescence of DMA between 300 and 500 nm (Fig. S2), or by measuring the DMA and DMA-O₂ using HPLC (Fig. S3) [27]. The method is now the widely adopted standard method to detect $^1\text{O}_2$ in nonaqueous electrochemical environments [17,27,28,30,31,54–56].

3.1. $^1\text{O}_2$ during Li-O₂ cell cycling containing catalysts

Composite electrodes were made as detailed in the Experimental Section using PTFE binder. They comprised either pure Super P carbon black (SP), hydrophilic Super P (SP hp), TiC nanoparticles, or SP decorated with α -MnO₂ nanorods, Co₃O₄ nanorods, or Pd nanoparticles. To monitor $^1\text{O}_2$ formation upon a full discharge/charge cycle, operando fluorescence with a setup as described previously was used [27]. Briefly, the cell was built inside a sealed O₂ filled quartz cuvette with magnetic stirrer. The working electrode was pasted onto a stainless steel grid, immersed into O₂-saturated TEGDME containing 0.1 M LiTFSI and 1.6×10^{-5} M DMA as the electrolyte. This concentration is best suited for operando fluorescence detection [27]. Reference and counter electrodes were Li_{1-x}FePO₄. Excitation and emission wavelengths were chosen according to the respective maxima (Fig. S2).

Fig. 1a and b show the voltage and the DMA concentration upon galvanostatic discharge and charge of the different electrodes in the operando fluorescence cell. In accord with previous results, there is much less $^1\text{O}_2$ formation (i.e., DMA consumption) during discharge compared to charge [27], which is also in accord with the relative amounts of side reactions during discharge and charge [57,58]. As soon as the cells were switched to charge, the $^1\text{O}_2$ formation increased substantially and kept increasing as the voltage rose. The $^1\text{O}_2$ formation shows a strong dependence on the electrode material. Pristine SP may be considered as a base case carbon electrode material and showed an integral $^1\text{O}_2$ formation over the discharge/charge cycle at the lower end of the observed range. Hydrophilic SP and TiC show larger amounts while MnO₂, Co₃O₄, and Pd show slightly smaller amounts.

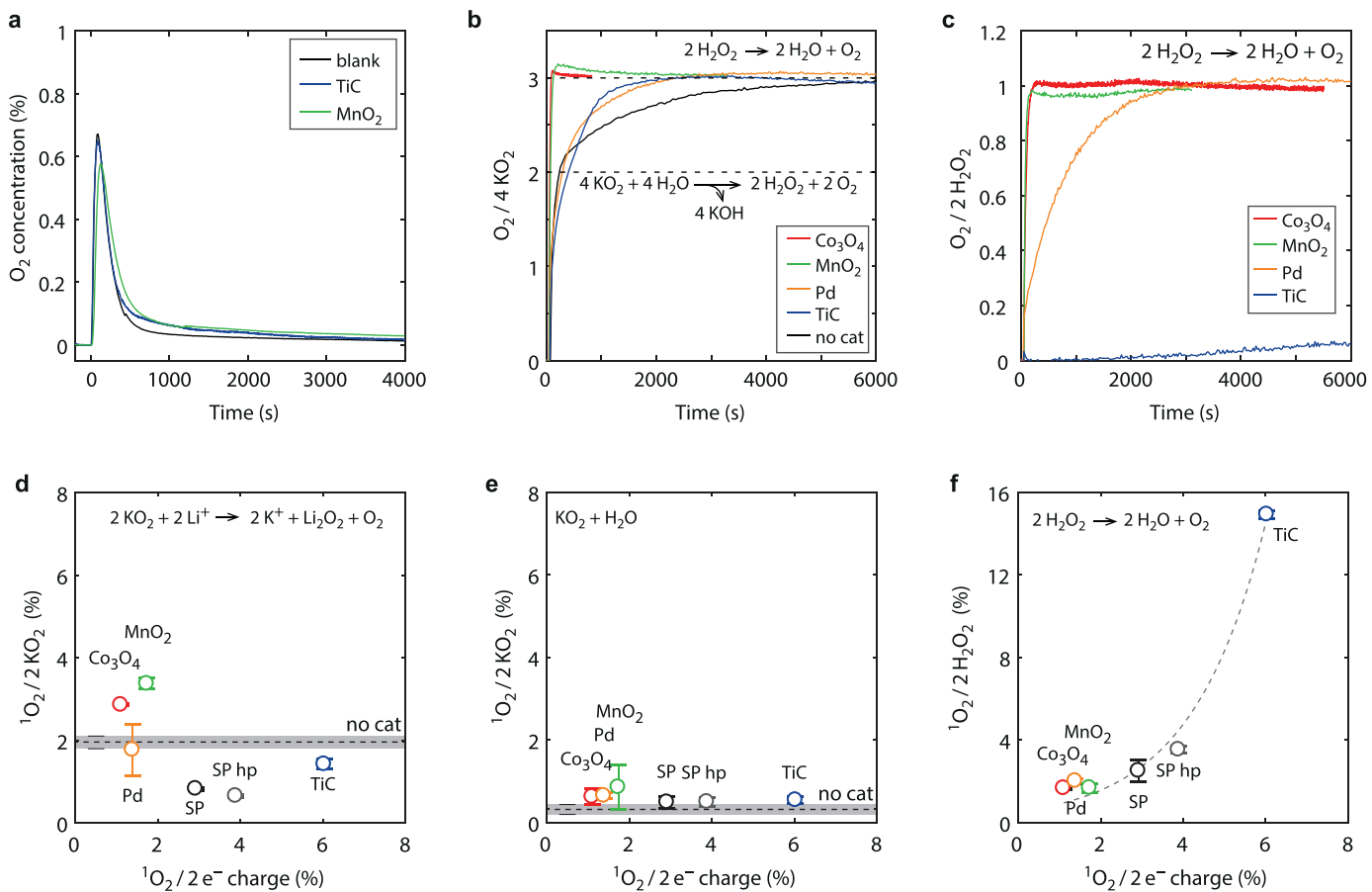


Fig. 2. Catalyst's influence on $^1\text{O}_2$ yield from individual reactions. (a) O_2 evolution (as measured by MS) versus time upon mixing KO_2 and the indicated catalyst with 0.1 M LiTFSI in TEGDME containing 30 mM DMA. (b) O_2 evolution (as measured by pressure increase) versus time upon mixing KO_2 and the indicated catalyst in TEGDME containing 30 mM DMA and 1000 ppm H_2O . (c) O_2 evolution versus time upon immersing the indicated catalyst in TEGDME containing 30 mM DMA, 170 mM H_2O_2 , and 3% H_2O . (d) Molar ratio of $^1\text{O}_2/2 \text{KO}_2$ formed during LiO_2 disproportionation in (a). (e) Molar ratio of $^1\text{O}_2/2 \text{KO}_2$ formed during proton assisted LiO_2 disproportionation in (b). (f) Molar ratio of $^1\text{O}_2/2 \text{H}_2\text{O}_2$ formed during H_2O_2 decomposition in (c). Values for SP, SP hp, and TiC are taken from Fig. 3. The dotted line is and exponential fit and to guide the eye. (d) to (f) are plotted as a function of $^1\text{O}_2/2 \text{e}^-$ upon charge (Fig. 1c), the same versus $^1\text{O}_2/2 \text{e}^-$ upon discharge is shown in Fig. S7.

To sensitively quantify $^1\text{O}_2$ formation upon discharge, we maximized sensitivity for $^1\text{O}_2$ using 30 mM DMA in the electrolyte, which is close to saturation. Sandwich cells with the same working, reference, and counter electrodes, and with an electrolyte soaked glass fibre separator were discharged to ~ 1 mAh, the electrolyte then extracted and analysed by HPLC. Fig. 1c shows the moles of $^1\text{O}_2$ per two moles electrons passed (*i.e.*, per O_2 reduced) on discharge and relates this value to the same quantity obtained on charge. Of note, moles of $^1\text{O}_2$ formed per mole of electrons passed on charge (as obtained from operando fluorescence) should not directly be compared with moles of $^1\text{O}_2$ formed per mole of electrons passed on discharge; the lower DMA concentration required for fluorescence causes lower sensitivity. The graph reveals the $^1\text{O}_2$ formation on charge and discharge to be directly proportional and catalysts that form little/much $^1\text{O}_2$ on discharge do the same on charge.

3.2. Deciphering the reaction steps where catalysts impact $^1\text{O}_2$ formation

Directly proportional $^1\text{O}_2$ formation on discharge and charge across the catalysts as shown in Fig. 1c suggests that (1) the reactions involved in $^1\text{O}_2$ formation to be the same on discharge/charge and (2) the decisive step(s) where the catalyst influences the $^1\text{O}_2$ yield is/are the same. We therefore decipher in the

following the responsible step(s) by isolating reaction steps and measuring the $^1\text{O}_2$ yields as a function of the catalyst present.

In the introduction, we summarized the known pathways to form $^1\text{O}_2$ in metal- O_2 cells to be superoxide disproportionation in presence of alkali cations or H^+ as well as H_2O_2 decomposition. Overall, catalysts could influence the $^1\text{O}_2$ formation in M- O_2 cells via their impact on three reactions



which we separately investigate in the following. Reactions were performed in a closed vessel as shown in Fig. S1 and O_2 evolution monitored by either MS or pressure increase. As superoxide source, we used KO_2 as a substitute for the thermodynamically unstable and in pure phase inaccessible LiO_2 . This is justified since we could show previously that solid micron sized KO_2 powder immersed into Li^+ electrolyte (TEGDME) was quantitatively converted to Li_2O_2 [28]. KO_2 will therefore first undergo ion exchange ($\text{KO}_2 + \text{Li}^+ \rightarrow \text{LiO}_2 + \text{K}^+$) and is hence a valid precursor for LiO_2 with minor influence of the presence of K^+ on the further behaviour of the LiO_2 .

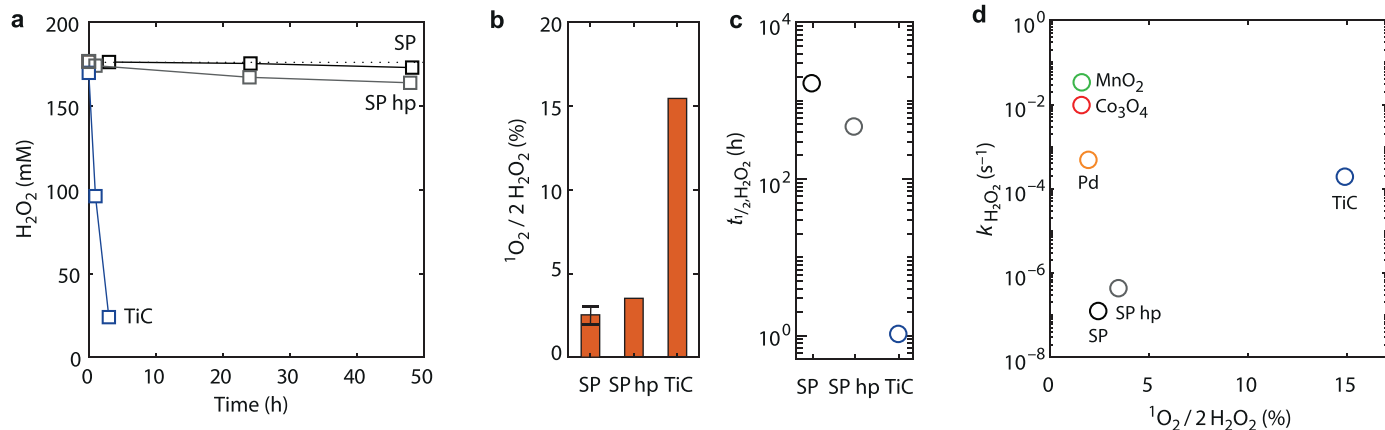


Fig. 3. (a) H_2O_2 concentration versus time upon mixing 170 mM H_2O_2 in TEGDME with the indicated catalyst. (b) Molar ratio of ${}^1\text{O}_2/2 \text{H}_2\text{O}_2$ taking into account the decomposed H_2O_2 in (a). (c) Half-life time $t_{1/2, \text{H}_2\text{O}_2}$ of H_2O_2 as obtained from the data in (a) and (b). (d) Kinetics of H_2O_2 decomposition $k_{\text{H}_2\text{O}_2}$ versus the fraction of ${}^1\text{O}_2$ relative to the decomposed H_2O_2 . Values for MnO_2 , Co_3O_4 , and Pd were obtained from Fig. 2c, values for the others from Fig. 3a. Values versus ${}^1\text{O}_2$ on discharge/charge are shown in Fig. S9.

Considering first LiO_2 disproportionation (Eq. (4)), Fig. 2a shows representative O_2 evolution over time as measured by MS upon mixing KO_2 and the catalyst powder with 0.1 M LiTFSI in TEGDME that contained 30 mM DMA. The amount of Li^+ and DMA was in excess to the KO_2 . After O_2 evolution ceased, the electrolyte was extracted and analysed by HPLC for the degree of DMA \rightarrow DMA- O_2 conversion. The this-way obtained moles of ${}^1\text{O}_2$ per two moles of KO_2 are shown in Fig. 2d for the different catalyst as a function of ${}^1\text{O}_2/2 \text{e}^-$ on charge (Fig. 1c). The same data plotted against ${}^1\text{O}_2/2 \text{e}^-$ on discharge is shown in Fig. S7a. In accord with previous results, LiO_2 disproportionation without a catalyst yielded $\sim 2\%$ ${}^1\text{O}_2$ (grey area) [28]. Presence of the conductors (SP, SP hp, Pd, TiC) generally suppressed ${}^1\text{O}_2$ to some extent while the oxides MnO_2 and Co_3O_4 increased it. This finding points at the underlying mechanisms: (1) Conductors may cause quenching of ${}^1\text{O}_2$, which forms upon the LiO_2 disproportionation [59,60]. (2) Catalytically active oxides with flexible oxidation states such as Co_3O_4 and MnO_2 may catalyse the singlet disproportionation pathway but not the triplet path. In this context we recall previous findings that LiO_2 disproportionation to Li_2O_2 and ${}^3\text{O}_2$ passes minor or no activation barriers [28,35,39,61], while the pathway to evolve ${}^1\text{O}_2$ involves a sizeable activation barrier [28,29]. The ratio of activation barriers is hence responsible for the ${}^3\text{O}_2/{}^1\text{O}_2$ ratio. With the catalyst predominantly acting on the singlet path, the larger ${}^1\text{O}_2$ fraction is explicable.

Turning to the proton assisted superoxide disproportionation (Eq. (5)), Fig. 2b shows the O_2 pressure rise over time in presence of the various catalysts when KO_2 is immersed in TEGDME containing 1000 ppm H_2O . KO_2 will in a first step exchange K^+ for H^+ to form KOH and HO_2 , which then disproportionates to H_2O_2 . H_2O_2 will further catalytically decompose to H_2O and O_2 both due to presence of the catalysts and the base OH^- [46]. The latter is seen for the case when no catalyst was present (black trace). Accordingly, the pressure rise (O_2 evolution) proceeds in two distinguishable steps: fast evolution of 2 $\text{O}_2/4 \text{KO}_2$ followed by slower evolution of one further $\text{O}_2/4 \text{KO}_2$ to a total of 3 $\text{O}_2/4 \text{KO}_2$. Given that H_2O_2 is stable in TEGDME/1000 ppm H_2O , H_2O_2 decomposition must be OH^- catalysed and can hence not be stopped in the present experiments with HO_2 forming from KO_2 and H_2O . Note that in Li^+ containing systems Li_2O_2 can precipitate in parallel [62]. Catalysts present accelerate both steps; somewhat with Pd and TiC as the catalysts and substantially with MnO_2 and Co_3O_4 as the catalysts.

Fig. 2e shows the associated ${}^1\text{O}_2$ formation for different catalyst as a function of the ${}^1\text{O}_2/2 \text{e}^-$ on charge (Fig. 1c). The same data plotted against the ${}^1\text{O}_2/2 \text{e}^-$ on discharge is shown in Fig. S7b. Uncatalysed HO_2 disproportionation forms in accord with previous findings a minor ${}^1\text{O}_2$ fraction, which is significantly below that from LiO_2 disproportionation [28,63,64]. Equally, OH^- catalysed H_2O_2 decomposition in TEGDME/1000 ppm H_2O is found to form minor ${}^1\text{O}_2$ in accord with previous findings in pure H_2O solution [47]. All solid catalysts increased the ${}^1\text{O}_2$ yield slightly yet close to error margins. Hence, presence of catalysts does not significantly change ${}^1\text{O}_2$ yields from proton mediated superoxide disproportionation, which rejects this step to be the step where catalysts impact ${}^1\text{O}_2$ formation on cycling.

Turning to catalysed H_2O_2 disproportionation (Eq. (6)), Fig. 2c shows the pressure rise over time when the various catalysts where mixed with 170 mM H_2O_2 in TEGDME containing 3% H_2O . While this experiment would not particularly require H_2O to be present, the H_2O content arose from the use of aqueous H_2O_2 solution to prepare the test solution. MnO_2 and Co_3O_4 fully decomposed the H_2O_2 within several minutes, whereas with Pd it took ~ 1 h and with TiC $\sim 8\%$ of the expected O_2 (based on initial H_2O_2) evolved after ~ 1.5 h. The carbons caused only minor O_2 evolution. Fig. 2f shows the associated ${}^1\text{O}_2$ formation for the different catalyst as a function of ${}^1\text{O}_2/2 \text{e}^-$ on charge (Fig. 1c). ${}^1\text{O}_2$ formation with the different catalyst as a function of ${}^1\text{O}_2/2 \text{e}^-$ on discharge is shown in Fig. S7c. There is a clear correlation between ${}^1\text{O}_2$ formation upon electrochemical cycling and upon H_2O_2 decomposition.

At this point it should be noted that H_2O_2 decomposition is not necessarily reliably measured by O_2 evolution (Fig. 2c) since reactive intermediates may react with the organic solvent and may then not evolve O_2 into the gas phase. When large fractions of ${}^1\text{O}_2$ form, O_2 evolution will underestimate H_2O_2 consumption and its measurement is inaccurate for very slow reactions such as with the carbons or TiC. To get quantifiable values for formed ${}^1\text{O}_2$ per decomposed H_2O_2 (i.e., ${}^1\text{O}_2/2 \text{H}_2\text{O}_2$), the carbons and TiC were brought into contact with $\text{H}_2\text{O}_2/\text{TEGDME}$ for up to 2 days. H_2O_2 consumption and ${}^1\text{O}_2$ were probed at certain sampling points as shown in Fig. 3a. TiC decomposed most of the H_2O_2 within several hours whilst forming a fraction of $\sim 15\%$ ${}^1\text{O}_2/2 \text{H}_2\text{O}_2$ based on the decomposed H_2O_2 (Fig. 3b). The carbons only decomposed a small fraction of the H_2O_2 within 2 days and formed ~ 2.5 and 3.5% ${}^1\text{O}_2/2 \text{H}_2\text{O}_2$ for SP and SP hp, respectively. Fig. 3c shows the time constants for H_2O_2 decomposition in terms of half-life time $t_{1/2, \text{H}_2\text{O}_2}$. The carbons have a $t_{1/2, \text{H}_2\text{O}_2}$ of ~ 500 and ~ 1700 h with

only 2.5 to 3.5% $^1\text{O}_2$ yield, which will generate close to negligible $^1\text{O}_2$ within the timespan of cycling of a couple of hours. In contrast, for TiC with its $t_{1/2, \text{H}_2\text{O}_2}$ of ~1 h, the H_2O_2 decomposition and associated $^1\text{O}_2$ generation of ~15% is relevant on the timescale of cycling. Overall, there is no simple trend between the rate of H_2O_2 decomposition by a catalyst and the $^1\text{O}_2$ yield therefrom as shown in Fig. 3d.

Mechanistically, the high fraction of $^1\text{O}_2$ from H_2O_2 decomposition with TiC may be explained with Ti^{IV} forming stable peroxy complexes [46] such as those used for detecting H_2O_2 using TiOSO_4 . Equally, Ti^{IV} -peroxy interactions catalysing $^1\text{O}_2$ from H_2O_2 are reasonable for solid surfaces and to release $^1\text{O}_2$ under spin conservation. Apart from TiC, other Ti ceramics have been proposed as Li-O₂ electrode materials and need to be treated with caution with regard to catalysing $^1\text{O}_2$ formation [22]. This applies more generally for transition metals of the groups 3 to 6 in d° configuration, which have been shown to evolve large amounts of $^1\text{O}_2$ when in contact with H_2O_2 [47]. In this vein also Mo^{VI} compounds are expected to evolve $^1\text{O}_2$ as seen with MoO_4^{2-} , which is a standard method to effectively produce $^1\text{O}_2$ from H_2O_2 [65]. So far Mo_2C [21] and MoS_2 [16] have been proposed with diametric conclusions. Mo_2C has shown very poor reversibility while MoS_2 was suggested to show good Li-O₂ performance. Note that group 6 compounds, even if inserted in reduced states, feature M^{VI} (M = Cr, Mo) surface terminations, particularly after being exposed to oxidizing potentials, as shown by XPS or XAS [19,21]. Hence, effective $^1\text{O}_2$ generation could be expected analogously to presence of MoO_4^{2-} . To test this, we brought a H_2O_2 solution in contact with MoS_2 and found ~17% $^1\text{O}_2$ following decently fast H_2O_2 decomposition (Fig. S10). Another pathway to form $^1\text{O}_2$ from H_2O_2 decomposition at transition metal oxides may set in when additionally Li^+ is present since superoxide was reported as intermediate [66], which will further give $^1\text{O}_2$ upon its disproportionation as shown above (Fig. 2a,d). Overall, transition metal compounds turn out to have to be used with caution as catalyst or electrode material as they feature multiple pathways to effectively catalyse $^1\text{O}_2$ formation in the Li-O₂ environment.

4. Conclusions

The impact of a representative selection of electrocatalysts and non-carbon electrode materials on $^1\text{O}_2$ formation during cycling of Li-O₂ cells has been measured and the reaction steps where the surfaces impact $^1\text{O}_2$ yields were deciphered. As a sensitive and selective probe for $^1\text{O}_2$, we used 9,10-dimethylanthracene (DMA) which forms the related endoperoxide (DMA-O₂) upon $^1\text{O}_2$ contact. Operando fluorescence and ex-situ HPLC analysis during cell cycling established that catalysts that cause small/large $^1\text{O}_2$ on discharge do the same proportionally on charge. This suggests the same $^1\text{O}_2$ formation mechanisms to act on discharge and charge. We deciphered the individual steps of the multi-step discharge/charge mechanism, where the catalysts impact the $^1\text{O}_2$ yields. Transition metal oxides raise $^1\text{O}_2$ yields upon LiO_2 disproportionation by suppressing the barrier of the singlet reaction path. The major correlation between $^1\text{O}_2$ yields on cycling was found with catalysed H_2O_2 decomposition. Transition metal compounds are generally prone to increase $^1\text{O}_2$. Judging the effect of catalyst on reversibility requires therefore a comprehensive set of metrics and particularly also to consider $^1\text{O}_2$ formation.

Declaration of Competing Interest

The authors declare that they have no known competing financial interests or personal relationships that could have appeared to influence the work reported in this paper.

CRedit authorship contribution statement

Aleksej Samojlov: Investigation, Visualization. **David Schuster:** Investigation, Visualization. **Jürgen Kahr:** Investigation. **Stefan A. Freunberger:** Conceptualization, Methodology, Validation, Investigation, Software, Resources, Data curation, Visualization, Writing - original draft, Writing - review & editing, Project administration, Funding acquisition.

Acknowledgments

S.A.F. thanks the International Society of Electrochemistry for awarding the Tajima Prize 2019 “in recognition of outstanding researches on Li-Air batteries by the use of a range of in-situ electrochemical methods to achieve comprehensive understanding of the reactions taking place at the oxygen electrode”. This article is dedicated to the special issue of *Electrochimica Acta* associated with the awarding conference. S.A.F. is indebted to and the Austrian Federal Ministry of Science, Research and Economy and the Austrian Research Promotion Agency (grant No. 845364) and the European Research Council (ERC) under the European Union’s Horizon 2020 research and innovation programme (grant agreement No 636069). The authors thank J. Schlegl for manufacturing instrumentation, M. Winkler of Acib GmbH and G. Strohmeier for help with HPLC measurements, S. Eder for cyclic voltammetry measurements, and C. Slugovc for discussions and continuous support. We thank S. Borisov for access and advice with fluorescence measurements. We thank EL-Cell GmbH, Hamburg, Germany for providing the PAT-Cell-Press electrochemical cell.

Supplementary materials

Supplementary material associated with this article can be found, in the online version, at doi:[10.1016/j.electacta.2020.137175](https://doi.org/10.1016/j.electacta.2020.137175).

References

- [1] D. Aurbach, B.D. McCloskey, L.F. Nazar, P.G. Bruce, Advances in understanding mechanisms underpinning lithium-air batteries, *Nat. Energy* 1 (2016) 16128.
- [2] S. Monaco, A.M. Arangio, F. Soavi, M. Mastragostino, E. Paillard, S. Passerini, An electrochemical study of oxygen reduction in pyrrolidinium-based ionic liquids for lithium/oxygen batteries, *Electrochim. Acta* 83 (2012) 94–104.
- [3] Y. Wang, Y.-C. Lu, Nonaqueous Lithium–Oxygen batteries: Reaction mechanism and critical open questions, *Energy Storage Materials* 28 (2020) 235–246.
- [4] I. Ruggieri, C. Arbizzani, F. Soavi, A novel concept of Semi-solid, Li Redox Flow Air (O_2) Battery: a breakthrough towards high energy and power batteries, *Electrochim. Acta* 206 (2016) 291–300.
- [5] H.-D. Lim, B. Lee, Y. Bae, H. Park, Y. Ko, H. Kim, J. Kim, K. Kang, Reaction chemistry in rechargeable Li-O₂ batteries, *Chem. Soc. Rev.* 46 (2017) 2873–2888.
- [6] W.-J. Kwak, H. Kim, H.-G. Jung, D. Aurbach, Y.-K. Sun, Review—A Comparative Evaluation of Redox Mediators for Li-O₂ Batteries: A Critical Review, *J. Electrochem. Soc.* 165 (2018) A2274–A2293.
- [7] C. Liu, M. Carboni, W.R. Brant, R. Pan, J. Hedman, J. Zhu, T. Gustafsson, R. Younesi, On the Stability of NaO_2 in Na-O₂ Batteries, *ACS Appl. Mater. Interf.* 10 (2018) 13534–13541.
- [8] X. Gao, Y. Chen, L. Johnson, P.G. Bruce, Promoting solution phase discharge in Li-O₂ batteries containing weakly solvating electrolyte solutions, *Nat. Mater.* 15 (2016) 882–888.
- [9] N.B. Aetukuri, B.D. McCloskey, J.M. García, L.E. Krupp, V. Viswanathan, A.C. Luntz, Solvating additives drive solution-mediated electrochemistry and enhance toroid growth in non-aqueous Li-O₂ batteries, *Nat. Chem.* 7 (2014) 50–56.
- [10] Y.-C. Lu, B.M. Gallant, D.G. Kwabi, J.R. Harding, R.R. Mitchell, M.S. Whittingham, Y. Shao-Horn, Lithium-oxygen batteries: bridging mechanistic understanding and battery performance, *Energy Environ. Sci.* 6 (2013) 750–768.
- [11] Y. Wang, N.-C. Lai, Y.-R. Lu, Y. Zhou, C.-L. Dong, Y.-C. Lu, A Solvent-Controlled Oxidation Mechanism of Li_2O_2 in Lithium–Oxygen Batteries, *Joule* 2 (2018) 2364–2380.
- [12] Z. Liang, Y.-C. Lu, Critical role of redox mediator in suppressing charging instabilities of lithium–oxygen batteries, *J. Am. Chem. Soc.* 138 (2016) 7574–7583.
- [13] T. Liu, G. Kim, M.T.L. Casford, C.P. Grey, Mechanistic Insights into the challenges of cycling a nonaqueous Na-O₂ battery, *J. Phys. Chem. Lett.* 7 (2016) 4841–4846.
- [14] R.A. Wong, C. Yang, A. Dutta, M. O, M. Hong, M.L. Thomas, K. Yamanaka, T. Ohta, K. Waki, H.R. Byon, Critically examining the role of nanocatalysts

- in Li-O₂ batteries: viability toward suppression of recharge overpotential, rechargeability, and cyclability, *ACS Energy Lett.* 3 (2018) 592–597.
- [15] N.-C. Lai, G. Cong, Z. Liang, Y.-C. Lu, A highly active oxygen evolution catalyst for lithium-oxygen batteries enabled by high-surface-energy facets, *Joule* 2 (2018) 1511–1521.
- [16] M. Asadi, B. Sayahpour, P. Abbasi, A.T. Ngo, K. Karis, J.R. Jokisaari, C. Liu, B. Narayanan, M. Gerard, P. Yasaei, X. Hu, A. Mukherjee, K.C. Lau, R.S. Assary, F. Khalili-Araghi, R.F. Klie, L.A. Curtiss, A. Salehi-Khojin, A lithium-oxygen battery with a long cycle life in an air-like atmosphere, *Nature* 555 (2018) 502.
- [17] N. Mahne, O. Fontaine, M.O. Thotiyil, M. Wilkening, S.A. Freunberger, Mechanism and performance of lithium-oxygen batteries – a perspective, *Chem. Sci.* 8 (2017) 6716–6729.
- [18] Y. Wang, Z. Liang, Q. Zou, G. Cong, Y.-C. Lu, Mechanistic insights into catalyst-assisted nonaqueous oxygen evolution reaction in lithium-oxygen batteries, *J. Phys. Chem. C* 120 (2016) 6459–6466.
- [19] K.P.C. Yao, M. Risch, S.Y. Sayed, Y.-L. Lee, J.R. Harding, A. Grimaud, N. Pour, Z. Xu, J. Zhou, A. Mansour, F. Barde, Y. Shao-Horn, Solid-state activation of Li₂O₂ oxidation kinetics and implications for Li-O₂ batteries, *Energy Environ. Sci.* 8 (2015) 2417–2426.
- [20] S. Ma, Y. Wu, J. Wang, Y. Zhang, Y. Zhang, X. Yan, Y. Wei, P. Liu, J. Wang, K. Jiang, S. Fan, Y. Xu, Z. Peng, Reversibility of noble metal-catalyzed aprotic Li-O₂ batteries, *Nano Letters* 15 (2015) 8084–8090.
- [21] D. Kundu, R. Black, B. Adams, K. Harrison, K. Zavadil, L.F. Nazar, Nanostructured metal carbides for aprotic Li-O₂ batteries: new insights into interfacial reactions and cathode stability, *J. Phys. Chem. Lett.* 6 (2015) 2252–2258.
- [22] D. Kundu, R. Black, E. Jamstorp, L. Nazar, A highly active nanostructured metallic oxide cathode for aprotic Li-O₂ batteries, *Energy Environ. Sci.* 8 (2014) 1292–1298.
- [23] B.D. McCloskey, R. Scheffler, A. Speidel, D.S. Bethune, R.M. Shelby, A.C. Luntz, On the efficacy of electrocatalysis in nonaqueous Li-O₂ batteries, *J. Am. Chem. Soc.* 133 (2011) 18038–18041.
- [24] J.-H. Kang, W.-J. Kwak, D. Aurbach, Y.-K. Sun, Sodium oxygen batteries: one step further with catalysis by ruthenium nanoparticles, *J. Mat. Chem. A* 5 (2017) 20678–20686.
- [25] S.A. Freunberger, Y. Chen, N.E. Drewett, L.J. Hardwick, F. Bardé, P.G. Bruce, The lithium-oxygen battery with ether-based electrolytes, *Angew. Chem. Int. Ed.* 50 (2011) 8609–8613.
- [26] J. Wandt, P. Jakes, J. Granwehr, H.A. Gasteiger, R.-A. Eichel, Singlet oxygen formation during the charging process of an aprotic lithium-oxygen battery, *Angew. Chem. Int. Ed.* 55 (2016) 6892–6895.
- [27] N. Mahne, B. Schafzahl, C. Leypold, M. Leypold, S. Grumm, A. Leitgeb, G.A. Strohmeier, M. Wilkening, O. Fontaine, D. Kramer, C. Slugovc, S.M. Borisov, S.A. Freunberger, Singlet oxygen generation as a major cause for parasitic reactions during cycling of aprotic lithium-oxygen batteries, *Nat. Energy* 2 (2017) 17036.
- [28] E. Mourad, Y.K. Petit, R. Spezia, A. Samojlov, F.F. Summa, C. Prehal, C. Leypold, N. Mahne, C. Slugovc, O. Fontaine, S. Brutt, S.A. Freunberger, Singlet oxygen from cation driven superoxide disproportionation and consequences for aprotic metal-O₂ batteries, *Energy Environ. Sci.* 12 (2019) 2559–2568.
- [29] A. Pierini, S. Brutt, E. Bodo, Superoxide Anion Disproportionation Induced by Li⁺ and H⁺: Pathways to ¹O₂ Release in Li-O₂ Batteries, *ChemPhysChem* (2020), doi:10.1002/cphc.202000318.
- [30] Z. Liang, Q. Zou, J. Xie, Y.-C. Lu, Suppressing singlet oxygen generation in lithium-oxygen batteries with redox mediators, *Energy Environ. Sci.* (2020).
- [31] L. Schafzahl, N. Mahne, B. Schafzahl, M. Wilkening, C. Slugovc, S.M. Borisov, S.A. Freunberger, Singlet oxygen during cycling of the aprotic sodium-O₂ battery, *Angew. Chem. Int. Ed.* 56 (2017) 15728–15732.
- [32] G. Houchins, V. Pande, V. Viswanathan, Mechanism for singlet oxygen production in Li-Ion and metal-air batteries, *ACS Energy Lett.* 5 (2020) 1893–1899.
- [33] S. Kang, Y. Mo, S.P. Ong, G. Ceder, A facile mechanism for recharging Li₂O₂ in Li-O₂ Batteries, *Chem. Mat.* 25 (2013) 3328–3336.
- [34] Y. Wang, Y.-R. Lu, C.-L. Dong, Y.-C. Lu, Critical factors controlling superoxide reactions in lithium-oxygen batteries, *ACS Energy Lett.* (2020) 1355–1363.
- [35] U. Das, K.C. Lau, P.C. Redfern, L.A. Curtiss, Structure and stability of lithium superoxide clusters and relevance to Li-O₂ batteries, *J. Phys. Chem. Lett.* 5 (2014) 813–819.
- [36] D. Zhai, H.-H. Wang, J. Yang, K.C. Lau, K. Li, L.A. Curtiss, K. Amine, Disproportionation in Li-O₂ batteries based on large surface area carbon cathode, *J. Am. Chem. Soc.* 135 (2013) 15364–15372.
- [37] C. Sheng, F. Yu, Y. Wu, Z. Peng, Y. Chen, Disproportionation of sodium superoxide in metal-air batteries, *Angew. Chem. Int. Ed.* 57 (2018) 9906–9910.
- [38] X. Zhang, L. Guo, L. Gan, Y. Zhang, J. Wang, L.R. Johnson, P.G. Bruce, Z. Peng, LiO₂ cryosynthesis and chemical/electrochemical reactivities, *J. Phys. Chem. Lett.* (2017) 2334–2338.
- [39] Y. Zhang, X. Zhang, J. Wang, W.C. McKee, Y. Xu, Z. Peng, Potential-dependent generation of O₂^{·-} and LiO₂ and their critical roles in O₂ reduction to Li₂O₂ in aprotic Li-O₂ batteries, *J. Phys. Chem. C* 120 (2016) 3690–3698.
- [40] D.H. Chin, G. Chiericato, E.J. Nanni, D.T. Sawyer, Proton-induced disproportionation of superoxide ion in aprotic media, *J. Am. Chem. Soc.* 104 (1982) 1296–1299.
- [41] A.U. Khan, Direct spectral evidence of the generation of singlet molecular oxygen (¹Δ_g) in the reaction of potassium superoxide with water, *J. Am. Chem. Soc.* 103 (1981) 6516–6517.
- [42] W.H. Koppenol, Reactions involving singlet oxygen and the superoxide anion, *Nature* 262 (1976) 420–421.
- [43] K.U. Schwenke, M. Metzger, T. Restle, M. Piana, H.A. Gasteiger, The Influence of water and protons on Li₂O₂ crystal growth in aprotic Li-O₂ Cells, *J. Electrochem. Soc.* 162 (2015) A573–A584.
- [44] K.U. Schwenke, S. Meini, X. Wu, H.A. Gasteiger, M. Piana, Stability of superoxide radicals in glyme solvents for non-aqueous Li-O₂ battery electrolytes, *Phys. Chem. Chem. Phys.* 15 (2013) 11830–11839.
- [45] V. Giordani, S.A. Freunberger, P.G. Bruce, J.-M. Tarascon, D. Larcher, H₂O₂ decomposition reaction as selecting tool for catalysts in Li-O₂ Cells, *Electrochim. Solid State Lett.* 13 (2010) A180–A183.
- [46] N. Wiberg, A.F. Holleman, E. Wiberg, *Inorganic Chemistry*, 1st ed., Academic Press, 2001.
- [47] J.M. Aubry, Search for singlet oxygen in the decomposition of hydrogen peroxide by mineral compounds in aqueous solutions, *J. Am. Chem. Soc.* 107 (1985) 5844–5849.
- [48] B. Schafzahl, E. Mourad, L. Schafzahl, Y.K. Petit, A.R. Raju, M.O. Thotiyil, M. Wilkening, C. Slugovc, S.A. Freunberger, Quantifying total superoxide, peroxide, and carbonaceous compounds in metal-O₂ batteries and the solid electrolyte interphase, *ACS Energy Lett.* 3 (2017) 170–176.
- [49] D. Lepage, C. Michot, G. Liang, M. Gauthier, S.B. Schougaard, A soft chemistry approach to coating of LiFePO₄ with a conducting polymer, *Angew. Chem. Int. Ed.* 50 (2011) 6884–6887.
- [50] Y. Li, B. Tan, Y. Wu, Mesoporous Co₃O₄ nanowire arrays for lithium ion batteries with high capacity and rate capability, *Nano Letters* 8 (2008) 265–270.
- [51] A. Débart, A. Paterson, J. Bao, P. Bruce, α-MnO nanowires: a catalyst for the O₂ electrode in rechargeable lithium batteries, *Angew. Chem. Int. Ed.* 47 (2008) 4521–4524.
- [52] S.M. Borisov, G. Nuss, W. Haas, R. Saf, M. Schmuck, I. Klimant, New NIR-emitting complexes of platinum(II) and palladium(II) with fluorinated benzoporphyrins, *J. Photochem. Photobiol. A* 201 (2009) 128–135.
- [53] N. Mahne, S.E. Renfrew, B.D. McCloskey, S.A. Freunberger, Electrochemical oxidation of lithium carbonate generates singlet oxygen, *Angew. Chem. Int. Ed.* 57 (2018) 5529–5533.
- [54] Y.K. Petit, C. Leypold, N. Mahne, E. Mourad, L. Schafzahl, C. Slugovc, S.M. Borisov, S.A. Freunberger, DABCOnium: An Efficient and High-Voltage Stable Singlet Oxygen Quencher for Metal-O₂ Cells, *Angew. Chem. Int. Ed.* 58 (2019) 6535–6539.
- [55] L. Schafzahl, N. Mahne, B. Schafzahl, M. Wilkening, C. Slugovc, S.M. Borisov, S.A. Freunberger, Singulett-sauerstoff in der aprotischen natrium-O₂-batterie, *Angew. Chem.* 129 (2017) 15934–15938.
- [56] D. Córdoba, H.B. Rodríguez, E.J. Calvo, Singlet oxygen formation during the oxygen reduction reaction in DMSO LiTFSI on lithium air battery carbon electrodes, *ChemistrySelect* 4 (2019) 12304–12307.
- [57] A.C. Luntz, B.D. McCloskey, Li-air batteries: Importance of singlet oxygen, *Nat. Energy* 2 (2017) 17056.
- [58] M.M. Ottakam Thotiyil, S.A. Freunberger, Z. Peng, P.G. Bruce, The carbon electrode in nonaqueous Li-O₂ Cells, *J. Am. Chem. Soc.* 135 (2013) 494–500.
- [59] S. Lebedkin, I. Kareev, F. Hennrich, M.M. Kappes, Efficient quenching of singlet oxygen via energy transfer to semiconducting single-walled carbon nanotubes, *J. Phys. Chem. C* 112 (2008) 16236–16239.
- [60] K. Yanagi, T. Okazaki, Y. Miyata, H. Kataura, Deactivation of singlet oxygen by single-wall carbon nanohorns, *Chem. Phys. Lett.* 431 (2006) 145–148.
- [61] V.S. Bryantsev, M. Blanco, F. Faglioni, Stability of lithium superoxide LiO₂ in the gas phase: computational study of dimerization and disproportionation reactions, *J. Phys. Chem. A* 114 (2010) 8165–8169.
- [62] Y. Qiao, S. Wu, J. Yi, Y. Sun, S. Guo, S. Yang, P. He, H. Zhou, From O₂^{·-} to HO₂^{·-}: reducing By-products and overpotential in Li-O₂ batteries by water addition, *Angew. Chem. Int. Ed.* 56 (2017) 4960–4964.
- [63] J.M. Aubry, J. Rigaudy, C. Ferradini, J. Puchault, Search for singlet oxygen in the disproportionation of superoxide anion, *J. Am. Chem. Soc.* 103 (1981) 4965–4966.
- [64] E.J. Nanni, R.R. Birge, L.M. Hubbard, M.M. Morrison, D.T. Sawyer, Oxidation and dismutation of superoxide ion solutions to molecular oxygen. Singlet vs. triplet state, *Inorg. Chem.* 20 (1981) 737–741.
- [65] P.R. Ogilby, Singlet oxygen: there is indeed something new under the sun, *Chem. Soc. Rev.* 39 (2010) 3181–3209.
- [66] E. Giannello, P. Rumori, F. Geobaldo, B. Fubini, M.C. Paganini, The interaction between hydrogen peroxide and metal oxides: EPR investigations, *Applied Magnetic Resonance* 10 (1996) 173–192.